

## Article

# Experimental and Simulation Study on Reducing the Liquid Film and Improving the Performance of a Carbon-Neutral Methanol Engine

Yongzhi Li <sup>1</sup>, Zhi Zhang <sup>1,\*</sup>, Haifeng Liu <sup>1,\*</sup>, Weide Chang <sup>1</sup>, Zanqiao Shu <sup>1</sup>, Hu Wang <sup>1</sup>, Zunqing Zheng <sup>1</sup>, Hua Zhao <sup>2</sup>, Xinyan Wang <sup>2</sup> and Mingfa Yao <sup>1,3</sup>

<sup>1</sup> State Key Laboratory of Engines, Tianjin University, Tianjin 300072, China; liyz@tju.edu.cn (Y.L.); wadechang12@163.com (W.C.); shuzanqiao@163.com (Z.S.); wang\_hu@tju.edu.cn (H.W.); zhengzunqing@tju.edu.cn (Z.Z.); y\_mingfa@tju.edu.cn (M.Y.)

<sup>2</sup> Center for Advanced Powertrain and Fuels, Brunel University London, Uxbridge UB8 3PH, UK; hua.zhao@brunel.ac.uk (H.Z.); xinyan.wang@brunel.ac.uk (X.W.)

<sup>3</sup> School of Civil and Transportation Engineering, Qinghai Minzu University, Xining 810000, China

\* Correspondence: zhangzhi@tju.edu.cn (Z.Z.); haifengliu@tju.edu.cn (H.L.)

**Abstract:** Methanol is a potential carbon-neutral fuel. It has a high latent heat of vaporization, making it difficult to achieve evaporation and mixing, and it is prone to forming a liquid film, which in turn affects engine performance. To reduce the liquid film and improve engine performance, this work investigates the influence mechanism of injection strategies on the generation of liquid films in the intake port and cylinder of an inline 6-cylinder port fuel injection (PFI) spark-ignition (SI) methanol engine and further explores the optimization scheme for improving engine performance. The results show that the end of injection (EOI) influences the methanol evaporation rate and the methanol–air mixing process, thereby determining the liquid film deposition, mixture distribution, and temperature distribution in the cylinder. As the EOI advances, the higher methanol evaporation rate during the intake process reduces the amount of methanol droplets and the deposition of a liquid film in the cylinder. The in-cylinder temperature is relatively high, while the mixture inhomogeneity slightly increases. As the EOI increases from 170 °CA to 360 °CA, the higher in-cylinder temperature and properly stratified mixture accelerate the early and middle stages of combustion, shorten the ignition delay, advance the center of combustion, and improve the brake thermal efficiency (BTE). However, further advancing the EOI results in the BTE remaining basically unchanged. Optimized injection timing can enhance the BTE by 1.4% to 2.4% under various load conditions. The increase in the EOI contributes to the reduction of HC emissions due to the weakening of the crevice effect with lower masses of methanol droplets and liquid film in the cylinder, while the increase in mixture inhomogeneity leads to an increase in CO emissions. In general, controlling the EOI at around 360 °CA can maintain relatively low CO emissions under various load conditions, while significantly reducing HC emissions by 71.2–76.4% and improving the BTE.

**Keywords:** methanol engine; liquid film formation; methanol evaporation mixing; combustion; emission



Academic Editor: Constantine D. Rakopoulos

Received: 21 December 2024

Revised: 11 January 2025

Accepted: 11 January 2025

Published: 15 January 2025

**Citation:** Li, Y.; Zhang, Z.; Liu, H.; Chang, W.; Shu, Z.; Wang, H.; Zheng, Z.; Zhao, H.; Wang, X.; Yao, M.

Experimental and Simulation Study on Reducing the Liquid Film and Improving the Performance of a Carbon-Neutral Methanol Engine.

*Energies* **2025**, *18*, 353. <https://doi.org/10.3390/en18020353>

**Copyright:** © 2025 by the authors.

Licensee MDPI, Basel, Switzerland.

This article is an open access article distributed under the terms and conditions of the Creative Commons Attribution (CC BY) license

(<https://creativecommons.org/licenses/by/4.0/>).

## 1. Introduction

In order to cope with the global energy and environmental pollution problems, the proposal of the “dual-carbon” goal puts forward a new development direction for the automobile industry, and reducing the carbon emissions of the powertrain has become an

important technical route [1,2]. Especially for the heavy-duty engines widely used in heavy-duty trucks and construction machinery. The rapid development of the transportation and infrastructure industries has led to a rapid increase in the demand for heavy-duty vehicles. Realizing fuel substitution for heavy-duty diesel engines is an important means of reducing carbon emissions and lessen the dependence on petroleum resources [3,4].

Recently, there has been rapid development in the technology of converting CO<sub>2</sub> into clean methanol liquid fuel using green hydrogen, on the basis of which methanol can be transformed from a low-carbon fuel to a carbon-neutral fuel, which is one of the most important ways to reduce carbon emissions in the future [5–7]. As a fuel, methanol has high economy, safety, environmental friendliness, reliability, and applicability, and is an ideal alternative fuel for traditional internal combustion engines, for which the modification cost will not increase significantly [8,9]. Moreover, methanol has a high octane number [10], high latent heat of vaporization [11], and high laminar flame speed [12]. A high octane number means good anti-knock performance, a high latent heat of vaporization can reduce the intake temperature, and a higher laminar flame speed can reduce the cycle-by-cycle variation. These properties allow the engine to use higher compression ratios to change the combustion characteristics and improve the thermal efficiency [13–15]. Moreover, methanol contains 50% oxygen and has no C-C bonds, which is favorable for reducing the CO, HC, and PM emissions produced during combustion [16,17].

Methanol has been studied and applied to both spark ignition (SI) and compression ignition (CI) engines. Due to the low cetane number of methanol [18], combined combustion with another highly reactive fuel is a common method of applying methanol to CI engines, such as diesel/methanol dual-fuel combustion, which is an effective method [19,20]. But the application of dual fuels greatly increases the complexity of the fuel supply system, electronic control system, and aftertreatment system [21]. On the contrary, methanol is well suited as a fuel for SI engines due to its high octane number, high volatility, and high latent heat of vaporization [22]. Methanol application in heavy-duty SI engines is a mature commercial approach and can easily reduce engine emissions when using the combustion scheme of stoichiometric combustion, exhaust gas recirculation (EGR), and three-way catalytic converter (TWCC) [23].

Güdden et al. [24] conducted combustion experiments on a port fuel injection (PFI) SI single-cylinder methanol engine and showed that the thermal efficiency of the methanol engine was higher than that of a natural gas engine. The NO<sub>x</sub> emissions met the International Maritime Organization (IMO) Tier III limits (<2 g/kWh), and there was no need for exhaust aftertreatment. However, the emissions of unburnt methanol, especially formaldehyde, were higher. Chen et al. [25] comparatively analyzed the combustion characteristics and cycle-by-cycle variations of methanol, ethanol, and n-butanol for SI engine combustion. They found that methanol had a higher combustion rate, lower cycle-by-cycle variation, and better lean combustion capability than ethanol and n-butanol. Gong et al. [26] used numerical simulation to investigate the effect of intake temperature on mixture formation, the combustion process, and the formaldehyde and unburned methanol emissions of a direct injection spark ignition (DISI) methanol engine. The results showed that increasing the intake temperature could promote the evaporation of methanol and improve the distribution of the mixture in the cylinder, which accelerated combustion and reduced the emissions of formaldehyde and unburned methanol. Duan et al. [27] conducted an experimental study on the effects of the injection timing and spark timing on the combustion and emission characteristics of a high compression ratio DISI methanol engine. They found that by optimizing the injection timing and spark timing, the cycle-by-cycle variation could be reduced, higher indicated mean effective pressure (IMEP) and indicated thermal efficiency (ITE) could be achieved, and the start of injection (SOI) was in the range of 270–240 °CA

BTDC for better combustion and emission performance. Li et al. [28] conducted an experimental study on the effects of SOI, spray angle, injection pressure, and spark timing on the in-cylinder flow, fuel distribution, flame propagation, and engine performance of a high compression ratio DISI methanol engine. They found that the combustion process was very sensitive to changes in the SOI, which was closely related to in-cylinder turbulence and methanol-air mixing. The injection pressure affected the combustion process mainly by influencing the in-cylinder methanol distribution. For steady combustion at low loads, a delayed SOI, narrower spray angles, and lower injection pressures are advised. Advancing the SOI improves the ITE and  $\text{NO}_x$  emissions at medium loads. Zhu et al. [29] investigated the effect of EGR rate and spark timing on BTE as well as the  $\text{NO}_x$ , CO, and HC emissions of a SI methanol engine. At the range of 1000–1700 rpm, the cycle-by-cycle variation was small, and the peak BTE was 41.4%, which was 3% higher than that of the original natural gas engine. It had lower  $\text{NO}_x$  and CO emissions but higher HC emissions. Moreover, the effects of injection pressure (8–24 MPa), injection timing (240–400 °CA BTDC), and excess air coefficient ( $\lambda = 1.1, 1.2$  and  $1.3$ ) on mixture formation and combustion performance were investigated by experiments and numerical simulations, and the results showed that the optimized injection strategy can improve the BTE by 2%, 2.7%, and 2.8% when the  $\lambda = 1.1, 1.2$ , and  $1.3$ , respectively [30].

Methanol performs well in SI engines and forming a higher quality mixture is critical for combustion and emission performance. However, after retrofitting a conventional fuel engine to a methanol engine, the corrosive wear of methanol on the engine structure also needs to be considered [31,32], especially in the piston ring and cylinder liner regions [33]. Related research mainly focuses on the improvement of lubrication system materials and engine corrosion treatment, and the corrosion wear can be mitigated by improving the methanol evaporation and methanol-air mixing process to reduce the formation of deposits. Since the latent heat of vaporization of methanol is significantly higher than that of gasoline, methanol injected at low pressure into the intake port is difficult to atomize and rapidly evaporate. A large number of methanol droplets entering the cylinder will lead to the formation of a liquid film. This may cause corrosion wear of the engine, incomplete combustion, and emissions, resulting in a reduction in engine performance. Therefore, it is necessary to thoroughly analyze the methanol evaporation characteristics, liquid film formation, and mixture formation of the methanol engine. The injection strategy plays a dominant role in the methanol-air mixing process and its influence on the mixture formation process is complex, influenced by engine structure, nozzle arrangement, and intake flow.

Based on the above literature review, it can be found that different injection strategies can influence the performance of methanol engines, which might be caused by the deposition of liquid films. Nevertheless, the shortcoming of current research is that the understanding of the mechanism of liquid film deposition is still not clear. To reduce the liquid film and improve engine performance, the paper experimentally investigates the effect of the injection timing on combustion and emission performance under different conditions based on a 14.8 L PFI SI methanol engine. Combined with three-dimensional simulation, the effect of the injection timing on the generation of a liquid film, methanol-air mixing process, and the mechanism of its influence on the combustion and emission characteristics is revealed. The results can provide a theoretical basis and guidance for controlling the injection parameters of PFI methanol engines.

## 2. Analytical Methodology

### 2.1. Experimental Setup

The experiments were performed in an inline 6-cylinder PFI SI methanol engine, as shown in Figure 1. Table 1 lists the basic technical parameters of the engine. The

methanol supply system adopted multipoint injection. An eddy current dynamometer with a maximum power of 630 kW and a maximum speed of 4500 rpm was used, with speed and torque accuracies of  $\pm 1$  rpm and  $\pm 0.3\%$  FS, respectively. An MT9020 methanol consumption meter, sourced from Changsha Hanzhou in China, was employed to measure the dynamic methanol consumption, with an accuracy of  $0.12\%$ FS. A thermal gas mass flow meter was used to measure air flow with an accuracy of  $\pm 0.1\%$  FS. Intake and exhaust pressures, temperatures, oil temperature, and pressure, as well as coolant temperature, were measured by pressure sensors and thermocouples with a temperature accuracy of  $\pm 1$  K and pressure accuracy of  $\pm 0.25\%$ . The in-cylinder pressure was measured by a Kistler cylinder pressure sensor from Shanghai, China. The combustion analysis system utilized a JH611 combustion analyzer developed by Hunan University, China, to continuously record the in-cylinder pressure curves for 200 consecutive cycles. Meanwhile, the crank angle data was collected at intervals of  $0.1^\circ$ CA. The emissions produced in the experiments included  $\text{NO}_x$ , CO, and HC, which were measured by the Horiba MEXA-7100DEGR device from Kyoto, Japan. The main measurements and their accuracy are listed in Table 2.

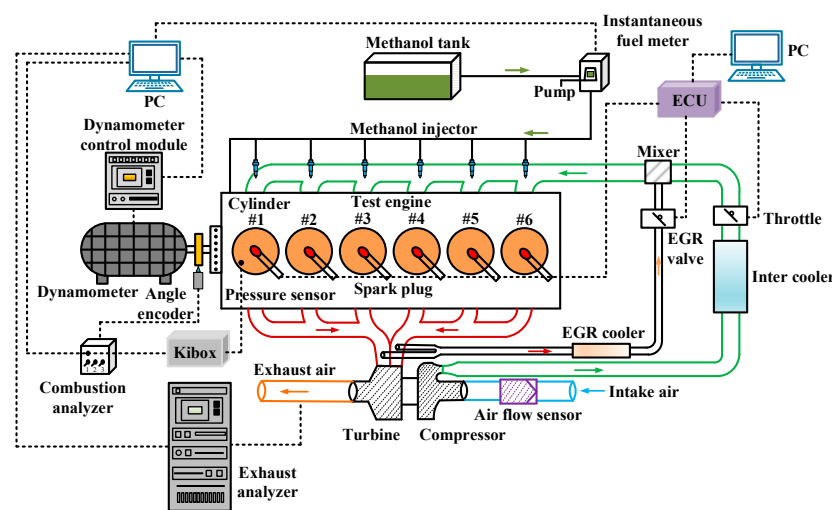


Figure 1. Schematic diagram of the test bench.

Table 1. Basic technical parameters of the methanol engine.

Parameters	Value
Engine type	6-cylinder, turbocharged, stoichiometric combustion
Bore/mm	138
Stroke/mm	165
Connecting rod/mm	244.5
Displacement/L	14.8
Compression ratio/-	13.5
Number of valves/-	4
Maximum power/(kW/rpm)	391/1700
Maximum torque/(N·m/rpm)	2600/(1000–1400)
Intake valve opening timing/ $^\circ$ CA BTDC	10
Intake valve closure timing/ $^\circ$ CA ABDC	59.5
Exhaust valve opening timing/ $^\circ$ CA BBDC	50
Exhaust valve closure timing/ $^\circ$ CA ATDC	12

## 2.2. Experimental Methodology

The test engine used a methanol injector with 16 holes and a nozzle diameter of 0.30 mm, and the static flow rate could reach 850 g/min at an operating pressure of 5 bar. The injection timing is represented by SOI and EOI, where the SOI is defined as the crank angle between the start of injection and the intake bottom dead center, and the EOI is defined as the crank angle between the end of injection and the intake bottom dead center. A larger EOI implies that the

injection ends earlier with respect to the intake valve opening timing (IVO). The phases of different injection timing and gas exchange processes are shown in Figure 2.

**Table 2.** Main measurements and accuracies.

Measurements	Measuring Range	Accuracy
Engine speed	0–4500 rpm	±1 rpm
Engine torque	0–3600 N·m	±0.3%
In-cylinder pressure	0–30 MPa	±0.5%
Air flow rate	0–2000 kg/h	±0.1%
Methanol flow rate	0–250 kg/h	±0.12%
Intake pressure	0–0.4 MPa	±0.25%
Intake temperature	0–150 °C	±1 K
Exhaust pressure	0–0.6 MPa	±0.25%
Exhaust temperature	0–1000 °C	±1 K
Crank angle	0–720 °CA	±0.1 °CA
CO emission	0–5000 ppm	±0.5%
HC emission	0–50,000 ppm	±0.5%
NO <sub>x</sub> emission	0–50,000 ppm	±0.5%

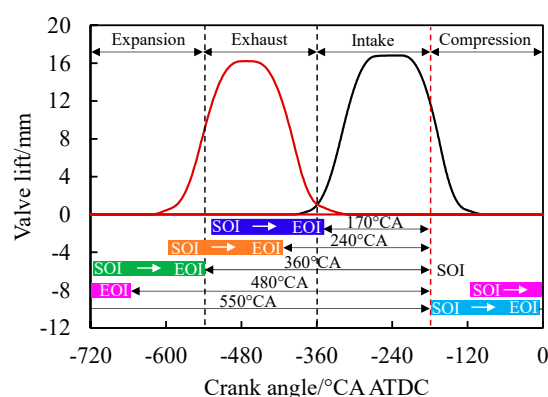


**Figure 2.** The injection timing and gas exchange phases.

The experiments were carried out under three different load conditions at 1400 rpm with IMEPs of 11.3 bar, 15.6 bar, and 19.6 bar. The injection pressures were controlled at around 6.5 bar. The injection duration and spark timing under the same conditions were consistent. Different injection timings were achieved by controlling the EOI, the minimum value of the EOI under different loads was 170 °CA, and the maximum value of the EOI was different, which was due to the fact that the test procedure attempted to control the completion of injection within the intake valve closing interval as much as possible. The experimental condition control parameters are listed in Table 3. The experimental results were measured under steady-state conditions and the collected data were averaged to obtain the final test data.

**Table 3.** Experimental condition control parameters.

Speed/(r/min)	IMEP/Bar	Intake Pressure After Intercooler/kPa	Intake Temperature After Intercooler/°C	EGR Rate/%	EOI/°CA	Injection Duration/°CA	Spark Timing/°CA BTDC
1400	11.3	165	35	14.0	170–550	170	−16.5
1400	15.6	200	40	17.8	170–420	230	−16.5
1400	19.6	235	45	17.5	170–360	330	−15.5

From the transient test results, the combustion phases could be determined and used to analyze the effect of the injection timing on the combustion rate at different stages. The combustion process was characterized using three parameters: the flame development period CA0–10, the combustion center CA50, and the rapid combustion period CA10–80. According to the combustion analysis results of the previous test, there was a lag phenomenon

in the heat release rate curve during the late combustion period, so CA10–80 was used to characterize the rapid combustion period. CA0–10 denotes the period from ignition to 10% cumulative heat release, CA50 indicates the point at 50% cumulative heat release, and CA10–80 signifies the phase from 10% to 80% cumulative heat release.

### 2.3. Numerical Study

#### 2.3.1. Computational Mesh and Models

The three-dimensional numerical model was established using Converge v2.4 software, as shown in Figure 3. Since the intake manifold is where the methanol injector is situated, the computational domain needed to include the manifold to prevent injected methanol from escaping. Additionally, due to the dynamic liquid film phenomenon in the intake port [34], the simulation required multi-cycle calculations. The purpose was to use the intake port state calculated in the previous cycle as the initial state of the current cycle, typically requiring more than 4–5 cycles of running. The mass of methanol in the cylinder must reach a stable value, which was regarded as a stable state in the simulation, as illustrated in Figure 4. The study calculated 9 cycles to ensure the accuracy of the simulation. The simulation calculations in this study were conducted on a simulation server equipped with 128 cores and 256 threads. A comprehensive multi-cycle calculation was carried out for the port fuel injection methanol engine. The computational time required for a single cycle calculation was approximately 30 h, and it required around 11 days to compute 9 cycles for one case.

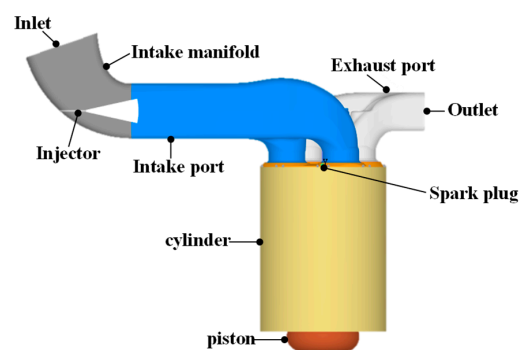


**Figure 3.** Three-dimensional numerical model.

Grid independence verification was carried out before the calculation, and the results are shown in Figure 5a; the base mesh size of the computational model was set to 4 mm. The meshes in the cylinder region were refined to 2 mm and 1 mm during the flow phase and combustion phases. The meshes around the injector were 0.5 mm. The grid sizes were 0.125 mm and 0.25 mm at the sphere region around the spark plug with radii of 2 mm and 4 mm, respectively. The meshes at the intake and exhaust valve cone angle area were refined to 0.5 mm to predict the intake and exhaust flow more precisely. The adaptive mesh refinement strategy based on velocity gradient (1 m/s) and temperature gradient (2.5 K) was also used, and 3 levels of adaptive refinement were applied to the intake port and cylinder region. The maximum number of meshes in the calculation process was about 2,500,000, and the specific mesh refinement regions and mesh size are shown in Figure 5b.

The numerical model used the Eulerian gas phase equation and the Lagrangian droplet equation to account for the phenomena of droplet breakup, evaporation, collision, and polymerization, as well as droplet attachment to the wall, liquid film stripping, and liquid film evaporation. The RNG  $k-\epsilon$  model was selected for the turbulence flow [35]. The KH-RT model was selected for the spray simulation [36]. The Frossling model was used to calculate the evaporation of droplets [37]. The No Time Counter (NTC) model was

selected for droplet collision [38]. The Wall film model was selected and coupled with the O'Rourke near-wall dynamics model to predict the spray-wall interaction process [39]. The heat transfer process was modeled by O'Rourke and Amsden [40], and the temperatures for each wall component are summarized in Table 4. The G-equation coupled with the chemical reaction kinetics model was used to capture the flame propagation process, and the methanol reaction mechanism used in this model contained 61 components and 479 reaction steps, which has been validated against a wide range of engine combustion conditions [41]. The computational efficiency of the SAGE chemistry solver was optimized by grouping similar computational grids with temperature differences up to 5 K and equivalence ratios up to 0.05 using the multi-zone model and calling the chemistry solver once for each group.

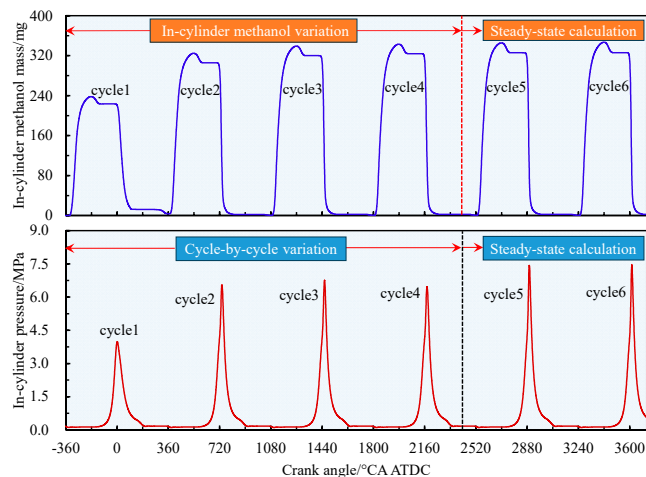


Figure 4. Methanol mass in the cylinder and cylinder pressure calculated by multi-cycle calculations.

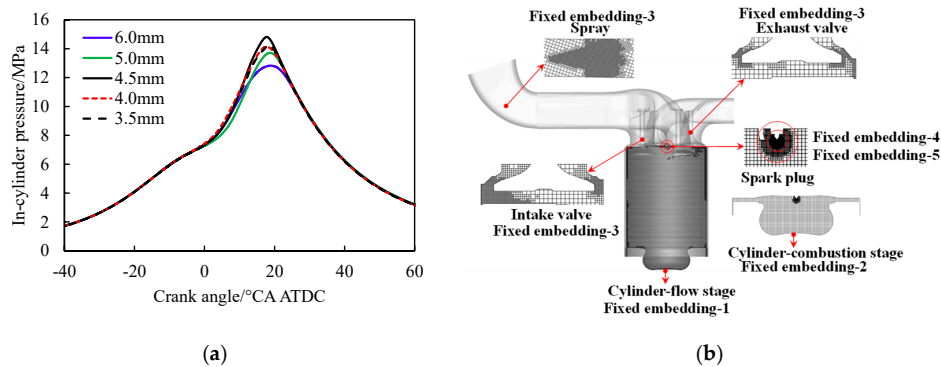


Figure 5. Grid independence and refinement strategies for the numerical model. (a) Grid independence. (b) Mesh refinement regions.

Table 4. Temperature values for different wall boundaries.

Wall Boundary Type	Temperature Value/K
Intake manifold	330
Intake port	360
Intake valve	450
Exhaust valve	525
Spark plug	600
Spark plug electrode	800
Cylinder head	500
Piston	550
Liner	450

### 2.3.2. Model Validation

The three-dimensional simulation calculations were performed at 1400 rpm and IMEP of 11.3 bar, and the in-cylinder pressures and heat release rates were investigated for five

different injection timings, with EOIs of 170 °CA, 240 °CA, 360 °CA, 480 °CA, and 550 °CA, respectively. The inlet and outlet boundaries, as well as the initial conditions of the model, were based on the measured data from the test bench. The specific operating parameters and boundary conditions entered into the model are shown in Table 5.

**Table 5.** Operational parameters and boundary conditions.

Parameters	Value
EGR rate/–	14.0%
Inlet pressure/MPa	0.125
Inlet temperatures/K	325
Methanol injection mass/(mg/cycle)	345
Number of holes/–	16
Nozzle diameter/mm	0.3
Spray cone angle/°	20
Injection pressure/bar	6.5
Injection duration/°CA	170
SOI/°CA	340, 410, 530, 650, 720
EOI/°CA	170, 240, 360, 480, 550
Spark timing/°CA ATDC	–16.5

The model validation results are shown in Figure 6. The black solid lines represent the average in-cylinder pressure for 100 cycles of the test, and the gray lines depict the in-cylinder pressure for each cycle. It is observed that good agreement was obtained between experiments and simulations in terms of both pressure traces and heat release rate profile. The maximum errors of CA10 and CA50 were within 2 °CA, and the maximum error of CA80 was within 3 °CA. This indicated that the methanol–air mixing process and flame propagation process of methanol in the cylinder could be precisely represented.

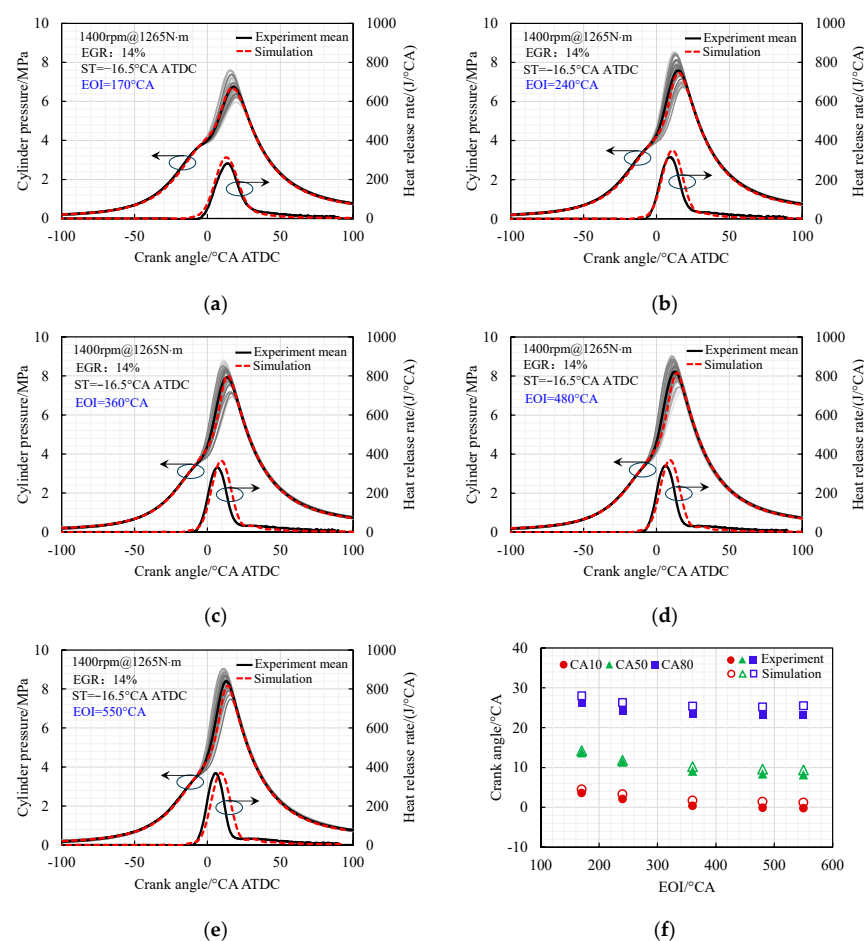


**Figure 6.** Verification results of simulation models under different injection timings. (a) EOI = 170 °CA. (b) EOI = 240 °CA. (c) EOI = 360 °CA. (d) EOI = 480 °CA. (e) EOI = 550 °CA. (f) Combustion phase.

### 3. Results and Discussion

#### 3.1. Effect of Injection Timing on the Methanol–Air Mixing Process

Figure 7 shows the mass fractions of the methanol vapor, droplets, and liquid film at IVO for the methanol injected at EOIs of 170 °CA, 240 °CA, 360 °CA, 480 °CA, and 550 °CA. As the EOI increases, the proportion of methanol vapor in the intake port gradually increases and the proportion of methanol droplets gradually decreases. When the EOI is 170 °CA, a large number of methanol droplets exist in the intake port, with a mass fraction of 0.76. However, when the EOI is 550 °CA, the mass fraction of the methanol droplets in the intake port decreases to 0.13, and the methanol with a mass fraction of 0.73 is vaporized. This is because a larger EOI will cause methanol to pre-mix in the intake port for a longer time, absorb more heat from the intake airflow and wall, and thus lead to a higher evaporation rate of methanol. Regarding the amount of methanol liquid film, as the EOI increases, the amount of methanol liquid film at the IVO first increases and then decreases. This is mainly because the change in the amount of liquid film within the intake port is a dynamic process. With the increase in the amount of methanol injection, the amount of liquid film gradually increases. From the end of injection to the time before the intake valve opens, during the dynamic process of further deposition and evaporation of the liquid film, the amount of liquid film gradually decreases after reaching its peak. This dynamic change process results in the amount of liquid film within the intake port under different EOIs presenting the abovementioned pattern.

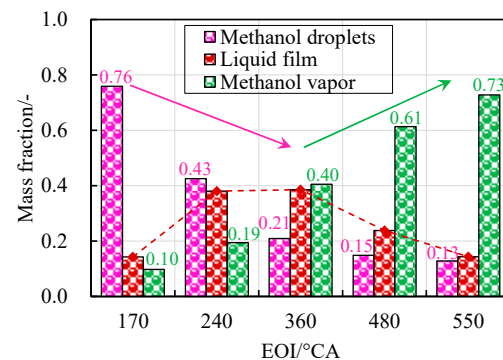


**Figure 7.** Mass fractions of methanol vapor, droplets, and liquid film in the intake port at the IVO for different EOIs.

To investigate the effect of the injection timing on the in-cylinder mixture preparation process, the variation in in-cylinder methanol charge and mixture homogeneity were analyzed, and the methanol charge coefficient  $C_f$  and the standard deviation of the excess air coefficient  $\lambda_{sd}$  were introduced to represent them quantitatively.  $C_f$  is defined as in Equation (1), where  $m_{cylinder}$  is the total mass of methanol entering the cylinder and  $m_{injection}$  is the methanol injection mass for the cycle. The definition of  $\lambda_{sd}$  is given in Equation (2), where  $m_{cell}$  is the mass of the mixture in each grid,  $\lambda_{cell}$  is the excess air coefficient in each grid,  $\lambda_{mean}$  is the average excess air coefficient in the cylinder, and  $m_{total}$  is the total mass of the mixture in the cylinder. A smaller  $\lambda_{sd}$  indicates a more homogeneous mixture in the cylinder [42].

$$C_f = \sqrt{\frac{m_{cylinder}}{m_{injection}}} \quad (1)$$

$$\lambda_{sd} = \sqrt{\frac{\sum_{cell} m_{cell} (\lambda_{cell} - \lambda_{mean})^2}{m_{total}}} \quad (2)$$

The evaporation and mixing process of methanol in the intake port directly affects the change in methanol charge in the cylinder after the IVO, which further influences the mixture formation process in the cylinder. Figure 8 shows the variation process of the intake mass flow rate,  $C_f$ , and  $\lambda_{sd}$  at different EOIs. The intake mass flow rates at different EOIs are essentially the same, and the growth rate of  $C_f$  shows an overall trend of rapid acceleration followed by deceleration. However, with the increase in EOI, the growth rate of the methanol charge in the early and middle stages of the intake stroke gradually accelerates, and then slows down in the later stage. At  $-300^\circ\text{CA}$  ATDC, EOIs of  $170^\circ\text{CA}$ ,  $240^\circ\text{CA}$ ,  $360^\circ\text{CA}$ ,  $480^\circ\text{CA}$ , and  $550^\circ\text{CA}$  correspond to  $C_f$  values of 0.56, 0.63, 0.72, 0.76, and 0.77, respectively. The crank angles corresponding to  $C_f$  reaching 0.90 at different EOIs are  $-251.4^\circ\text{CA}$  ATDC,  $-262.2^\circ\text{CA}$  ATDC,  $-276.6^\circ\text{CA}$  ATDC,  $-284.1^\circ\text{CA}$  ATDC, and  $-285.5^\circ\text{CA}$  ATDC, respectively. The aforementioned phenomenon is mostly caused by the following: in the early and middle stages of the intake stroke, the larger EOI causes more methanol in the intake port to evaporate into the gas phase, resulting in a faster growth rate of  $C_f$ ; in the late stage of the intake stroke, the growth rate is significantly slowed down by a small amount of methanol droplets that are still in the intake port, as well as methanol vapor from the evaporation of the liquid film entering the cylinder. When the EOI is  $170^\circ\text{CA}$ , the methanol in the intake port evaporation time is shorter and it mostly exists in the liquid phase at the IVO. Meanwhile, some of the methanol droplets in the intake process will continue to contact the wall to form a liquid film as they move with the air flow, and ultimately the methanol charge will be mixed while evaporating as it enters the cylinder, resulting in a relatively flat growth rate of  $C_f$ .

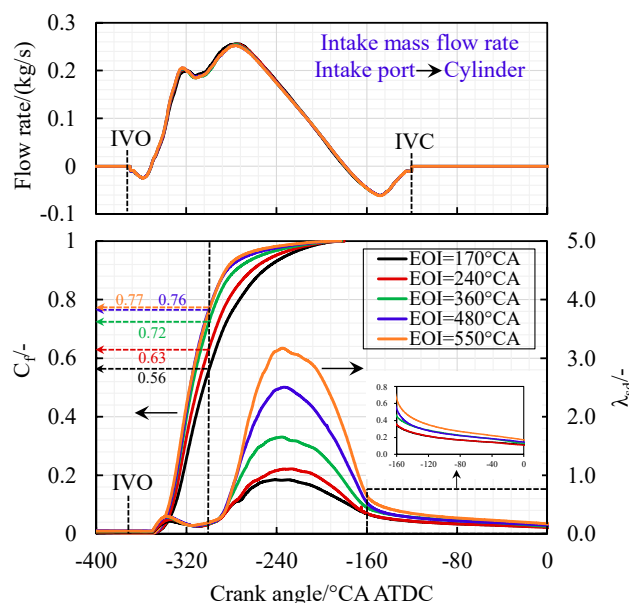
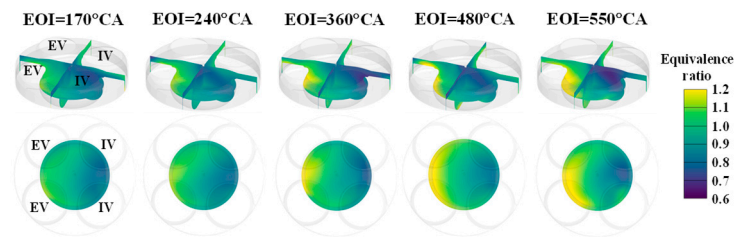


**Figure 8.** Variation process of intake mass flow rate,  $C_f$ , and  $\lambda_{sd}$  at different EOIs.

The change process of the in-cylinder methanol charge has a significant effect on the mixture formation process, as shown by the change in  $\lambda_{sd}$  in Figure 8. As EOI increases,  $\lambda_{sd}$  increases during the intake stroke. This is because in the early and middle stages of the intake stroke, the rapid growth in the methanol charge in the cylinder leads to a large amount of rich mixture entering the cylinder, resulting in an increase in mixture inhomogeneity. In the later stage, the lean mixture gradually enters the cylinder and mixes with the rich mixture, further increasing the inhomogeneity of the mixture. However, the difference in  $\lambda_{sd}$  at various EOIs decreases significantly during the subsequent compression

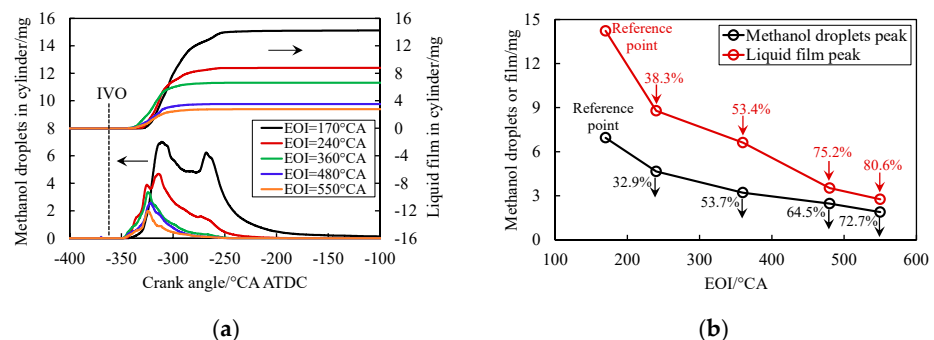
stroke, and finally the mixture inhomogeneity at the spark timing remains slightly higher as the EOI increases.

Figure 9 shows the distribution of in-cylinder mixture equivalent ratios for different EOIs at the spark timing. The in-cylinder mixture distributions all show a certain stratification phenomenon, with a lean mixture near the spark plug, a relatively rich mixture in the combustion chamber pit area, and a slightly higher mixture concentration on the exhaust side than on the intake side. As the EOI increases from 170 °CA to 550 °CA, the difference in mixture concentration near the spark plug is small, while the overall inhomogeneity of the in-cylinder mixture slightly increases. The stratification of the mixture between the intake side and the exhaust side gradually becomes more obvious, and more mixture is distributed on the exhaust side.



**Figure 9.** Equivalence ratio distributions of the mixture at the spark timing for different EOIs.

Figure 10 shows the change process of methanol droplets and liquid film mass in the cylinder during the intake process at different EOIs. It can be observed that when the EOI is 170 °CA, due to the relatively low evaporation rate of methanol in the intake port, a large number of methanol droplets enters the cylinder along with the airflow. Among them, a portion of droplets with a relatively larger mass forms a wall-attached liquid film after impacting the cylinder liner and piston under the action of the centrifugal force of the rotating airflow in the cylinder. With the increase in EOI, the masses of the in-cylinder methanol droplets and liquid film gradually decrease, and the time of in-cylinder methanol droplet existence is significantly shortened. Compared with an EOI of 170 °CA, the corresponding peaks of the methanol droplets in the cylinder at EOIs of 240 °CA, 360 °CA, 480 °CA, and 550 °CA decrease by 32.9%, 53.7%, 64.5%, and 72.7%, respectively. Additionally, the peak of the liquid film in the cylinder decreases by 38.3%, 53.4%, 75.2%, and 80.6%.



**Figure 10.** Variation in methanol droplet and liquid film masses in the cylinder at different EOIs. (a) Methanol droplet and liquid film masses. (b) Peak masses of methanol droplets and liquid film.

Figures 11 and 12 show the distribution of methanol droplets in the cylinder and the thickness of the liquid film adhered to the liner during the intake stroke at different EOIs, respectively. There are relatively more large-diameter methanol droplets near the wall of the intake port. This is mainly due to the high latent heat of vaporization of methanol. A large number of methanol spray droplets adhere to the intake port to form a liquid film. In

the process of methanol spray entering the cylinder, along with the interaction with the air flow, the methanol droplets absorb heat from the intake air and gradually evaporate, and the number of methanol droplets in the cylinder gradually decreases with the downward movement of the piston. The injection timing has a significant impact on the distribution of methanol droplets and liquid film in the cylinder. When the EOI is 170 °CA, there are more methanol droplets in the cylinder and some large droplets with a radius greater than 30  $\mu\text{m}$ . The thickness and distribution area of the liquid film in the cylinder are larger. As the EOI increases, the amount of methanol droplets, droplet radius, liquid film thickness, and liquid film distribution area in the cylinder gradually decrease. When the EOIs are 360 °CA, 480 °CA, and 550 °CA at  $-240$  °CA ATDC, the methanol droplets and liquid film in the cylinder basically evaporate.

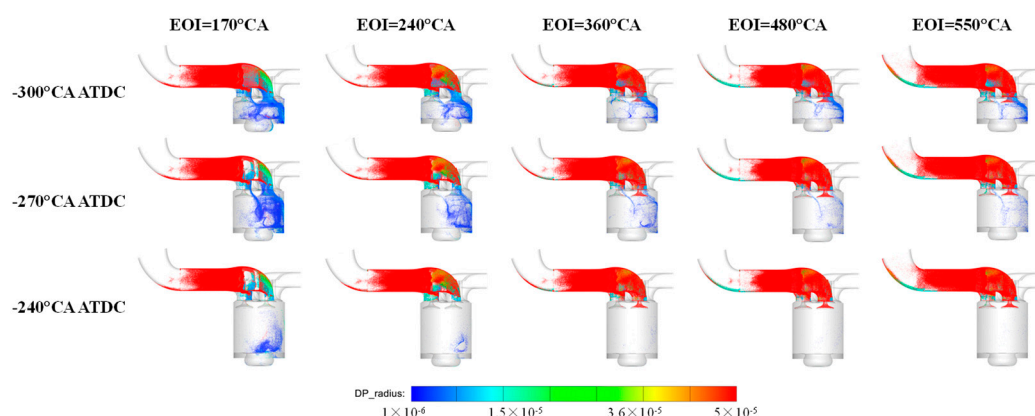


**Figure 11.** Distribution of methanol droplets in the cylinder during intake stroke at different EOIs.

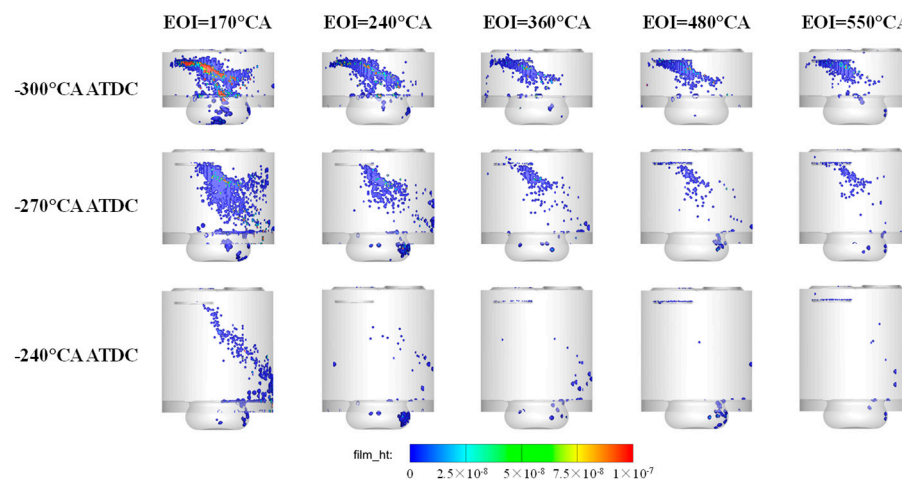


**Figure 12.** In-cylinder liquid film thickness during intake stroke at different EOIs.

According to the above analysis, the injection timing affects the change in methanol charge in the cylinder after the IVO, which influences the process of mixture formation in the cylinder. In addition, the injection timing will cause different phase states of methanol upon entering the cylinder after the IVO, thereby affecting the temperature distribution in the cylinder. Figure 13 shows the average in-cylinder temperatures at different EOIs obtained from the simulations. In the process of mixture formation, the in-cylinder temperature gradually increases with increasing EOI, especially from an EOI of 170 °CA to an EOI of 240 °CA. Ultimately, compared with an EOI of 170 °CA, at EOIs of 240 °CA, 360 °CA, 480 °CA, and 550 °CA, the in-cylinder temperatures at the spark timing increases by 6.5 K, 8.3 K, 10.3 K, and 10.7 K, respectively. This is due to the higher latent heat of vaporization

of methanol, as the injected methanol droplets absorb heat from the airflow and the wall in the intake port to evaporate. As the EOI increases, the evaporation rate of methanol before the IVO increases, as shown in Figure 7 above, and more methanol droplets absorb heat from the wall, causing the masses of the methanol droplets and the liquid film in the cylinder to decrease, as shown in Figure 10 above. This weakens the cooling effect of the evaporation of methanol droplets and the liquid film in the cylinder on the charge during the process [43].

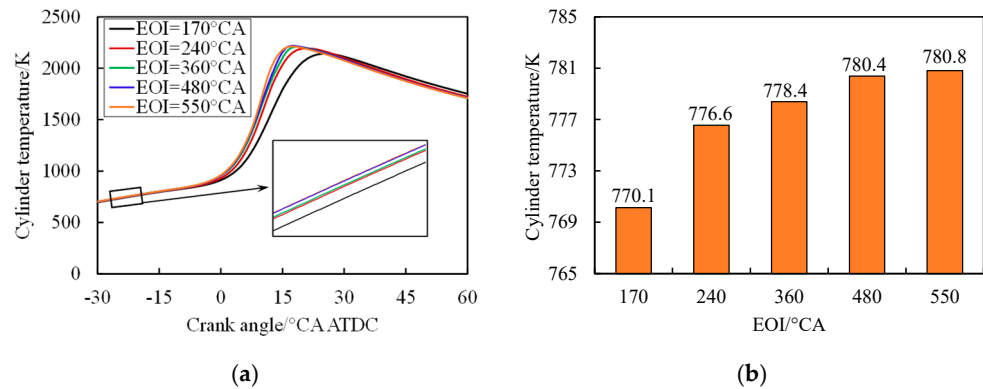


**Figure 13.** In-cylinder temperature at different EOIs. (a) In-cylinder temperature. (b) In-cylinder temperature at the spark timing.

Figure 14 shows the effect of the injection timing on the in-cylinder temperature distribution at the spark timing. It can be seen that the temperature distribution in the cylinder at different EOIs shows a certain gradient. The surrounding area has a high temperature, the middle area has a low temperature, and the exhaust side has a higher temperature than the intake side. When the EOI is 170 °CA, the overall temperature in the cylinder is low and the distribution is relatively uniform. As the EOI increases, the overall in-cylinder temperature increases, and the temperature increase in the combustion chamber space on the exhaust side is more pronounced.

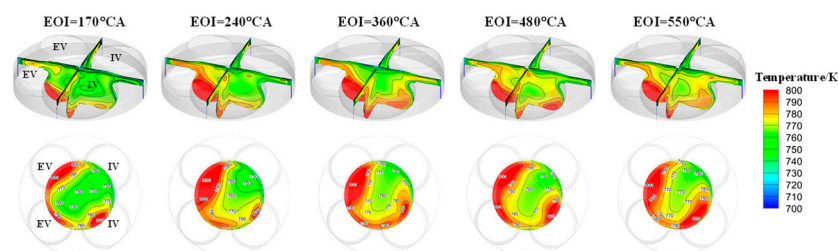


**Figure 14.** In-cylinder temperature distribution at the spark timing for different EOIs.

The above results show that the injection timing has a significant effect on the methanol–air mixing process. As the EOI increases from 170 °CA to 550 °CA, on the one hand, the evaporation rate of methanol in the intake port increases. A large amount of rich mixture enters the cylinder in the early and middle stages of the intake stroke, and a small amount of lean mixture gradually enters the cylinder in the later stage and mixes with the rich mixture. This leads to a slightly increased inhomogeneity of the mixture and more distribution of the mixture on the exhaust side. On the other hand, the methanol droplets absorb more heat from the wall of the intake port and evaporate, which obviously reduces the masses of the methanol droplets and liquid film in the cylinder, weakened the cooling effect on the charge during the evaporation of methanol droplets and liquid film, and the temperature in the cylinder increases.

### 3.2. Effect of Injection Timing on Combustion Performance

Figure 15 shows the effect of the injection timing on the cylinder pressure and heat release rate for different loads at 1400 rpm. The peak cylinder pressure and the peak heat release rate show increasing trends with increasing EOI, and the crank angle corresponding to the peak is advanced. At the IMEP condition of 11.3 bar, when the EOI increases from 170 °CA to 360 °CA, the increases in the peak of cylinder pressure and heat release rate are more obvious, and the phase corresponding to the peaks is significantly advanced. However, when the EOI continues to increase, the increase in peak values decreases, and the phase change corresponding to the peaks also decreases.

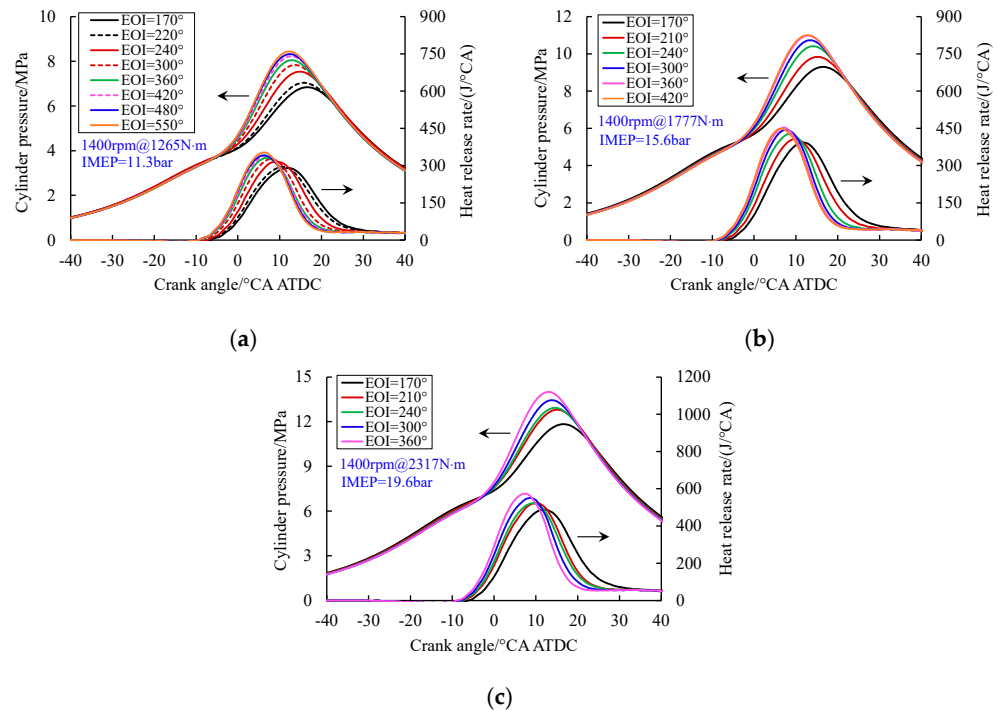


**Figure 15.** In-cylinder pressure and heat release rate at different EOIs for various conditions. (a) 1400 rpm, IMEP = 11.3 bar. (b) 1400 rpm, IMEP = 15.6 bar. (c) 1400 rpm, IMEP = 19.6 bar.

Based on the results of the cylinder pressure and heat release rate, the cumulative heat release rate was calculated by combustion analysis, and the combustion phase corresponding to each condition was obtained by combining with the spark timing. Figure 16 shows the effect of the injection timing on the combustion phase at 1400 rpm and an IMEP of 11.3 bar. It can be observed that when the EOI increases from 170 °CA to 360 °CA, compared with an EOI of 170 °CA, CA<sub>0–10</sub> is shortened by 1.5 °CA and 3.2 °CA, respectively. When the EOI continues to increase to 480 °CA and 550 °CA, CA<sub>0–10</sub> is slightly shortened. For CA<sub>50</sub>, as the EOI increases, CA<sub>50</sub> is advanced and combustion is closer to the top dead center. CA<sub>50</sub> is advanced by 2.3 °CA to 5.5 °CA. Meanwhile, it can be seen that after the EOI is 360 °CA, further increasing the EOI leads to a significant weakening of the trend of CA<sub>50</sub> advancement. CA<sub>10–80</sub> at different EOIs is generally closer and longer when the EOI is increased to 480 °CA and 550 °CA.

To further investigate the influence mechanism of the injection timing on combustion performance, the in-cylinder combustion process was analyzed in conjunction with the simulation results. Figure 17 shows the effect of the injection timing on the flame propagation in the cylinder during the combustion process at 1400 rpm and an IMEP of 11.3 bar, from which it can be seen that the flame propagation process and velocity change with the crank angle. At different EOIs, the flame propagation process in the cylinder is relatively

similar, and the development of the flame structure is asymmetric. The development speed along the exhaust side is much greater than that toward the intake side, which is mainly determined by the mixture distribution, temperature distribution, and turbulent kinetic energy distribution in the cylinder. The in-cylinder mixture distribution and temperature distribution are shown in Figures 9 and 14 above, and the turbulent kinetic energy distribution is shown in Figure 18.

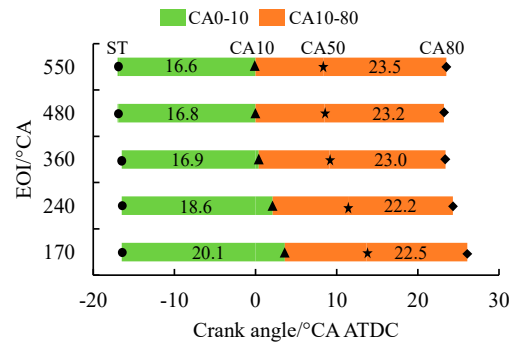


Figure 16. Combustion phases at 1400 rpm and IMEP of 11.3 bar with different EOIs.

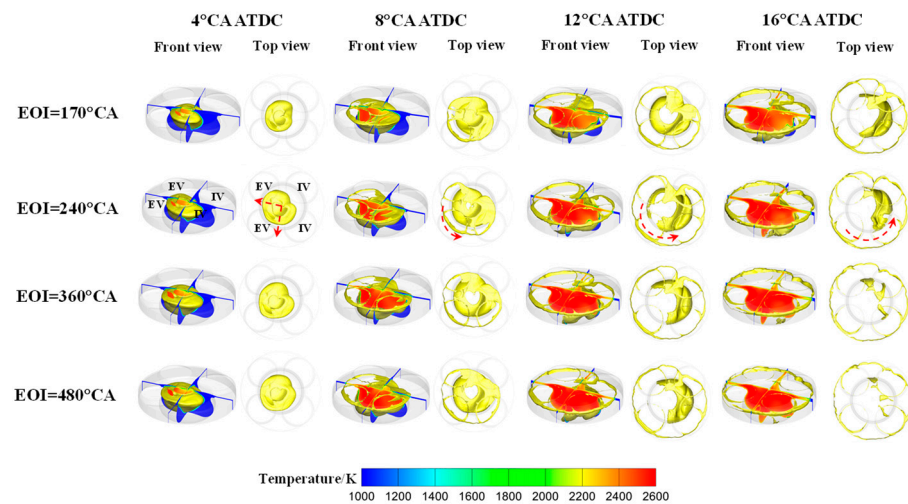


Figure 17. In-cylinder flame propagation (1800 K temperature iso-surface) at different EOIs.

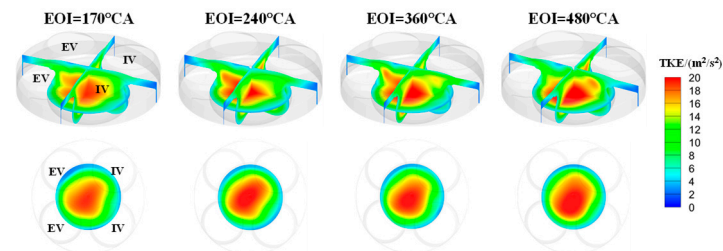


Figure 18. Turbulent kinetic energy distribution in the cylinder at the spark timing.

It can be observed that the area with a relatively high in-cylinder equivalence ratio and temperature is mainly on the exhaust side. Moreover, the area with a relatively high turbulent kinetic energy distribution is also mainly located at the center of the combustion chamber, biased towards the exhaust side. The above reasons jointly determine the development of the in-cylinder flame structure and indicate that combustion is mainly directed toward the exhaust side in the early and middle stages. After the combustion of the mixture on the exhaust side is complete, under the effect of the in-cylinder swirl flow, the mixture on the intake side of the combustion chamber is gradually exhausted in the middle and late

stages. Since the injection timing has little effect on the intake flow process, it has little effect on the turbulent kinetic energy in the cylinder. Therefore, the effect of the injection timing on the combustion process mainly depends on the equivalence ratio and temperature distribution in the cylinder. According to the simulation results, different injection timings have a relatively small effect on the equivalence ratio near the spark plug. As the EOI increases, the in-cylinder temperature is higher, which is conducive to improving the initial flame propagation speed and shortening CA0–10. As the EOI increases, the concentration of the mixture on the exhaust side increases, and the equivalence ratio of the mixture is mainly distributed around 1.1. The laminar flame speed of a moderately rich mixture is higher [20,44,45]. At the same time, accompanied by a higher in-cylinder temperature, it accelerates the early and middle stages of combustion and advances CA50. However, when the EOI continues to increase, the mixture concentration on the intake side becomes leaner, which has a negative impact on the middle and late stages of combustion. This leads to a reduced combustion rate, resulting in a small or even prolonged difference between CA10 and CA80.

Figure 19 shows the effect of the injection timing on brake-specific fuel consumption (BSFC) and BTE for different loads at 1400 rpm. It can be seen that as the load increases, the BSFC decreases and the BTE increases. As the EOI increases, the BSFCs under different loads all show the trend of first decreasing significantly and then remaining basically unchanged, and the trend in the BTE is opposite to that in the BSFC. At an IMEP of 11.3 bar, when the EOI increases from 170 °CA to 360 °CA, the BSFC is reduced by 16.2 g/kW·h, and the BTE is improved by 1.3%, and the BSFC and the BTE are basically unchanged by further increasing the EOI. According to the above analysis of the in-cylinder combustion process, this is due to the increase in EOI from 170 °CA to 360 °CA, the increase in cylinder temperature, and the appropriate increase in mixture concentration on the exhaust side. These factors significantly shorten CA0–10, advance CA50, bring combustion closer to the top dead center, and shorten the combustion duration, which contributes to the improvement of the BTE. Combined with the exhaust temperatures at different EOIs shown in Figure 20, as the EOI increases, the exhaust temperature gradually decreases and the heat carried by the exhaust is reduced, which is conducive to the piston work. However, when the EOI is further increased, although the exhaust temperature is still lower and the exhaust loss is smaller, the inhomogeneity of the mixture in the cylinder increases significantly. The change in CA50 is not obvious. The lean mixture on the intake side slows down the combustion rate in the middle and late stages, resulting in an extension of the overall combustion duration. At the same time, the higher in-cylinder temperature leads to increases in combustion and heat transfer losses, which hinders a further improvement in the BTE.

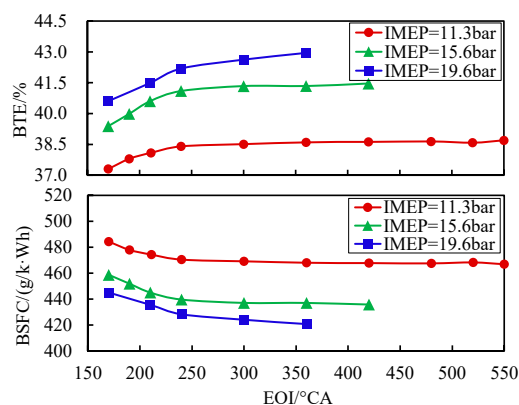
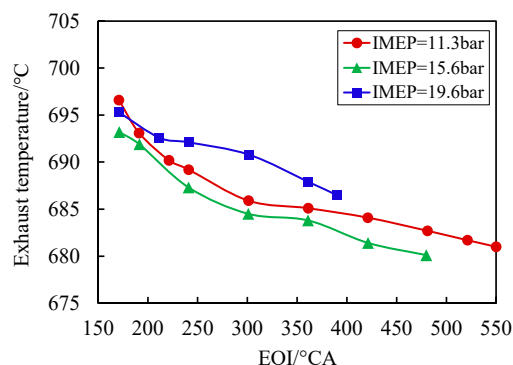


Figure 19. BSFC and BTE at different EOIs for various loads at 1400 rpm.



**Figure 20.** Exhaust temperature at different EOIs for various loads at 1400 rpm.

### 3.3. Effect of Injection Timing on Emission Characteristics

#### 3.3.1. CO Emissions

Figure 21 shows the effect of the injection timing on CO emissions at different loads of 1400 rpm. At an IMEP of 11.3 bar, the CO emissions basically show an increasing trend with the increase in EOI. The CO emissions mainly depend on the equivalence ratio of the mixture. When the fuel and air are not evenly mixed, the local mixture concentration is high, and the oxidation is incomplete due to insufficient combustion time, it will lead to higher CO emissions [27,46]. From the simulation results, it can be seen that an increase in the EOI increases the mixture inhomogeneity in the cylinder, raises CO generation, and simultaneously hinders CO post-oxidation due to lower exhaust temperatures [15], leading to an upward trend in CO emissions. When the EOI is 360 °CA, a further increase in the EOI leads to a significant increase in CO emissions. For IMEPs of 15.6 bar and 19.6 bar, with the gradual increase in EOI from 170 °CA, the CO emissions first decrease slightly and then increase significantly. This might be due to the increase in load, which greatly extends the injection duration of methanol. When the EOI increases from 170 °CA to 200 °CA, the range of change is small. It has a relatively minor impact on the in-cylinder mixture formation process. Eventually, the influence on CO emissions is not obvious. However, as the EOI increases, the overall trend in CO emissions is still gradually increasing.

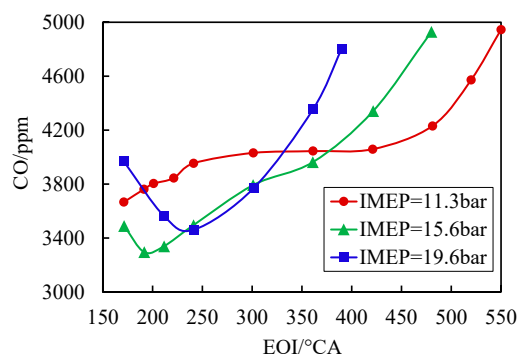


**Figure 21.** CO emissions at different EOIs for various loads at 1400 rpm.

To further investigate the influence mechanism of the injection timing on emission performance, the in-cylinder CO formation process was analyzed according to the simulation results. Figures 22 and 23 show the in-cylinder CO mass fraction and CO distribution at different injection timings. It can be seen that the CO generation region is mainly distributed in the region of the high mixture equivalence ratio. The CO mass fraction peaks around 15 °CA ATDC and then gradually decreases under the effect of combustion and oxidation. As the EOI increases, the peak value of CO mass fraction is higher. Moreover, it

remains relatively high during the subsequent oxidation process, leading to an increase in the final CO emissions.

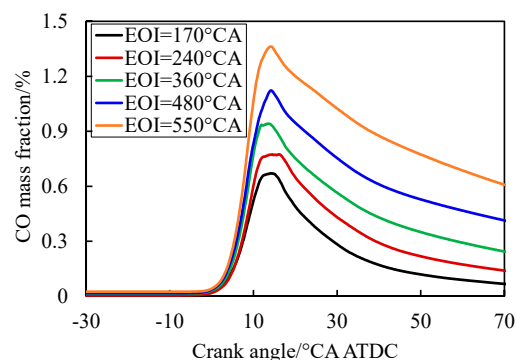


**Figure 22.** CO mass fraction in the cylinder during combustion at different EOIs.

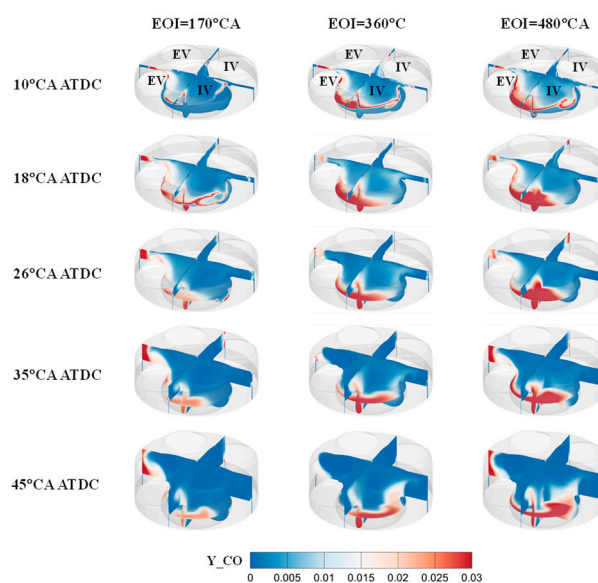


**Figure 23.** CO distribution in the cylinder during combustion at different EOIs.

### 3.3.2. HC Emissions

Figure 24 shows the effect of the injection timing on HC emissions for different loads at 1400 rpm. Incomplete combustion, quenching of the flame by the cold walls, and the crevice effect are the main reasons for HC emissions in SI engines [46,47]. It can be observed that as the load increases, the HC emissions increase. This is because under high-load conditions there is a greater injection mass and a longer injection duration. The evaporation rate of methanol in the intake port is lower, and more methanol droplets enter the cylinder. Under the centrifugal force of the airflow, the mass of methanol entering the piston crevices increases, thus leading to more HC emissions.

As the EOI increases, the HC emissions at different loads show a tendency to first decrease significantly and then level off. When the EOI is 360 °CA, the maximum reductions in HC emissions under various loads are 75.4%, 76.4%, and 71.2% respectively. Figure 25 shows the methanol mass distribution in the cylinder before the spark timing and during combustion with EOIs of 170 °CA, 360 °CA, and 480 °CA for an IMEP of 11.3 bar. As the EOI increases, the high methanol evaporation rate in the intake port leads to reductions in methanol droplets and liquid film in the cylinder. This reduces the mixture in the piston crevices and consequently results in a significant reduction in HC emissions. However, when the EOI is too large, as shown in Figures 10–12, the reductions in the masses of

methanol droplets and liquid film in the cylinder are significantly decreased, which weakens the reduction effect on HC emissions. Moreover, the concentration stratification in the cylinder becomes more obvious. The mixture concentration on the intake side near the edge of the combustion chamber is too lean, and the exhaust temperature is relatively low. This is not conducive to the HC oxidation process in the late stage of combustion. The combined effect of these two reasons makes the HC emissions show a basically flat trend.

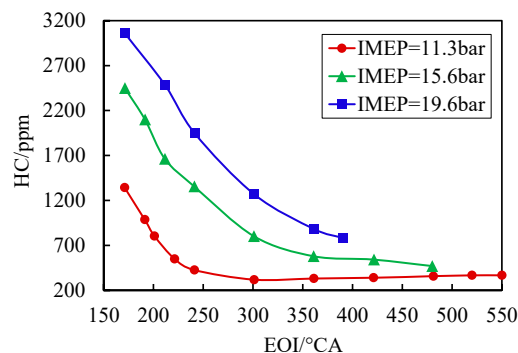


**Figure 24.** HC emissions at different EOIs for various loads at 1400 rpm.

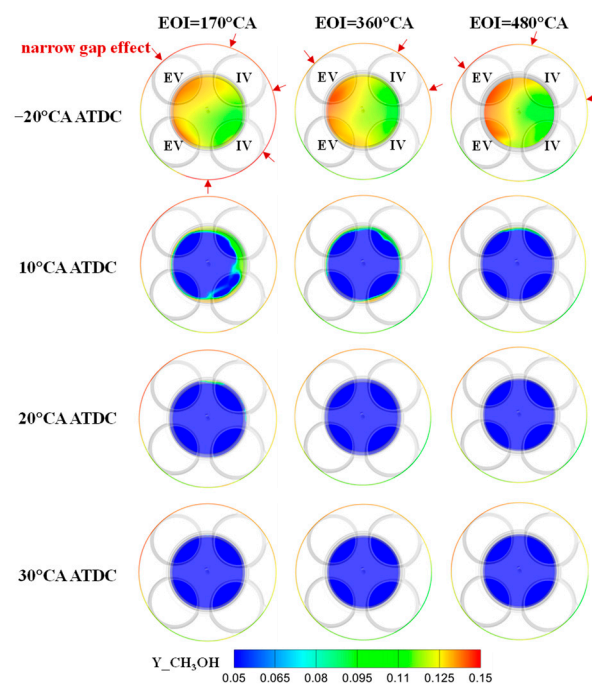


**Figure 25.** Mass fractions of methanol in the cylinder before the spark timing and during combustion at different EOIs.

#### 4. Conclusions

In this work, the effect of the injection timing on combustion and emission performance has been explored experimentally in a PFI SI methanol engine. The methanol evaporation characteristics, liquid film formation, and methanol–air mixing process under different injection timings, as well as their influence mechanisms on combustion and emission performance, were investigated through simulation. Innovatively, a comprehensive and detailed study of a PFI methanol engine was carried out via the multi-cycle simulation calculation method. The simulation model was fully verified based on the experimental data, and the mixture formation process was accurately visualized using CFD. The research findings can offer excellent theoretical guidance for the design of the injection system and the control of injection parameters in PFI methanol engines, aiming to reduce liquid

film deposition, improve the evaporation and mixing processes, boost thermal efficiency, and cut emissions, thereby enhancing the overall performance of the engine. The main conclusions are as follows:

- (1) The simulation results indicate that the injection timing directly influences the methanol–air mixing process and determines the in-cylinder liquid film deposition amount, mixture distribution, and temperature distribution. As the EOI increases, the evaporation rate of methanol in the intake port is enhanced, leading to reductions in the amounts of methanol droplets and liquid film in the cylinder. This weakens the cooling effect of methanol evaporation on the intake charge, resulting in a relatively high in-cylinder temperature.
- (2) The experimental results indicate that when the EOI is appropriately increased, the higher in-cylinder temperature and the properly stratified mixture accelerate the combustion rate in the early and middle stages, CA<sub>0–10</sub> is shortened, CA<sub>50</sub> is significantly advanced, and BTE is improved. When the EOI is further increased, the thinner mixture on the intake side slows down the middle and late stage combustion rates, which limits further improvement of the BTE.
- (3) Regarding emission performance, as the EOI increases, the amount of methanol in the piston crevices decreases. The weakening of the crevice effect leads to a reduction in HC emissions. However, the inhomogeneity of the in-cylinder mixture slightly increases, and the relatively low exhaust temperature weakens the post-oxidation process of CO, resulting in an increase in CO emissions.
- (4) A proper injection interval has better comprehensive performance. Controlling the EOI at approximately 360 °CA can maintain relatively low CO emissions under various load conditions. At the same time, it can significantly reduce HC emissions by 71.2–76.4% and increase the BTE by 1.3–2.4%.

Furthermore, the improvement of the overall performance of methanol engines demands a more favorable evaporation and mixing process. A large amount of methanol liquid film deposition can also lead to severe corrosion and wear, thus reducing reliability. The position, injection direction, and injection pressure of the methanol injector in the intake port all require further optimization research. Moreover, well-designed intake port and combustion chamber structures can also directionally transport methanol into the cylinder, so as to improve the mixture preparation process.

**Author Contributions:** Conceptualization, Y.L.; Data curation, W.C.; Investigation, H.L., Z.S., H.W., Z.Z. (Zunqing Zheng) and H.Z.; Methodology, Y.L. and Z.Z. (Zhi Zhang); Project administration, M.Y.; Resources, H.L.; Validation, Z.Z. (Zhi Zhang); Writing—original draft, Y.L. and Z.Z. (Zhi Zhang); Writing—review & editing, H.L., X.W. and M.Y. All authors have read and agreed to the published version of the manuscript.

**Funding:** This work was funded by National Key R&D Program of China (No. 2023YFE0115300).

**Data Availability Statement:** The original contributions presented in the study are included in the article; further inquiries can be directed to the corresponding author.

**Conflicts of Interest:** The authors declare that they have no known competing financial interests or personal relationships that could have appeared to influence the work reported in this paper.

## Abbreviations

The following abbreviations are used in this manuscript:

PFI	Port fuel injection
SI	Spark ignition

SOI	Start of injection
EOI	End of injection
BTE	Brake thermal efficiency
CI	Compression ignition
TWCC	Three-way catalytic converter
EGR	Exhaust gas recirculation
DISI	Direct injection spark ignition
IMEP	Indicated mean effective pressure
ITE	Indicated thermal efficiency
IVO	Intake valve opening
BSFC	Brake-specific fuel consumption

## References

- Krishnan, M.G.; Rajkumar, S.; Thangaraja, J.; Devarajan, Y. Exploring the synergistic potential of higher alcohols and biodiesel in blended and dual fuel combustion modes in diesel engines: A comprehensive review. *Sustain. Chem. Pharm.* **2023**, *35*, 101180. [CrossRef]
- Reitz, R.D.; Ogawa, H.; Payri, R.; Fansler, T.; Kokjohn, S.; Moriyoshi, Y.; Agarwal, A.K.; Arcoumanis, D.; Assanis, D.; Bae, C.; et al. IJER editorial: The future of the internal combustion engine. *Int. J. Engine Res.* **2019**, *21*, 3–10. [CrossRef]
- Rakopoulos, C.D.; Rakopoulos, D.C.; Kosmadakis, G.M.; Papagiannakis, R.G. Experimental comparative assessment of butanol or ethanol diesel-fuel extenders impact on combustion features, cyclic irregularity, and regulated emissions balance in heavy-duty diesel engine. *Energy* **2019**, *174*, 1145–1157. [CrossRef]
- Ramsay, C.J.; Dinesh, K.K.J.R. Numerical modelling of a heavy-duty diesel-hydrogen dual-fuel engine with late high pressure hydrogen direct injection and diesel pilot. *Int. J. Hydrog. Energy* **2024**, *49*, 674–696. [CrossRef]
- Santasalo, A.A.; Nyari, J.; Wojciesz, M. Application of Synthetic Renewable Methanol to Power the Future Propulsion. SAE Technical Paper 2020-01-2151. 2020. Available online: <https://www.sae.org/publications/technical-papers/content/2020-01-2151/> (accessed on 20 December 2024).
- Pellegrini, L.A.; Soave, G.; Gamba, S.; Langè, S. Economic analysis of a combined energy–methanol production plant. *Appl. Energy* **2011**, *88*, 4891–4897. [CrossRef]
- Lonis, F.; Tola, V.; Cau, G. Assessment of integrated energy systems for the production and use of renewable methanol by water electrolysis and CO<sub>2</sub> hydrogenation. *Fuel* **2021**, *285*, 119160. [CrossRef]
- Di Iorio, S.; Catapano, F.; Magno, A.; Sementa, P.; Vaglietto, B.M. The Potential of Ethanol/Methanol Blends as Renewable Fuels for DI SI Engines. *Energies* **2023**, *16*, 2791. [CrossRef]
- Kumar Prajapati, L.; Vachan Tirkey, J.; Raj, R.; Jena, P.; Giri, A. Performance analysis of methanol fuelled SI engine with boosted intake pressure and LIVC: A thermodynamic simulation and optimization approach. *Appl. Therm. Eng.* **2024**, *252*, 123604. [CrossRef]
- Nathan Prasad, B.S.; Pandey, J.K.; Kumar, G.N. Impact of changing compression ratio on engine characteristics of an SI engine fueled with equi-volume blend of methanol and gasoline. *Energy* **2020**, *191*, 116605. [CrossRef]
- Ricci, F.; Mariani, F.; Papi, S.; Zemi, J.; Battistoni, M.; Grimaldi, C.N. The Synergy between Methanol M100 and Plasma-Assisted Ignition System PAI to Achieve Increasingly Leaner Mixtures in a Single-Cylinder Engine. *Energies* **2024**, *17*, 1659. [CrossRef]
- Katoch, A.; Asad, M.; Minaev, S.; Kumar, S. Measurement of laminar burning velocities of methanol–air mixtures at elevated temperatures. *Fuel* **2016**, *182*, 57–63. [CrossRef]
- Gong, C.; Yi, L.; Zhang, Z.; Sun, J.; Liu, F. Assessment of ultra-lean burn characteristics for a stratified-charge direct-injection spark-ignition methanol engine under different high compression ratios. *Appl. Energy* **2020**, *261*, 114478. [CrossRef]
- Sarıkoç, S. Environmental and enviro-economic effect analysis of hydrogen-methanol-gasoline addition into an SI engine. *Fuel* **2023**, *344*, 128124. [CrossRef]
- Zhang, B.; Chen, Y.; Jiang, Y.; Lu, W.; Liu, W. Effect of compression ratio and Miller cycle on performance of methanol engine under medium and low loads. *Fuel* **2023**, *351*, 128985. [CrossRef]
- Farooq, S.; Vinay Kumar, D. Experimental investigation of gasoline ethanol methanol iso-stoichiometric blends on SI engine. *Mater. Today Proc.* **2023**. [CrossRef]
- Sathish Kumar, T.; Ashok, B. Development of combustion control map for flex fuel operation in methanol powered direct injection SI engine. *Energy* **2024**, *288*, 129695. [CrossRef]
- Shamun, S.; Haşimoğlu, C.; Murcak, A.; Andersson, Ö.; Tunér, M.; Tunestål, P. Experimental investigation of methanol compression ignition in a high compression ratio HD engine using a Box-Behnken design. *Fuel* **2017**, *209*, 624–633. [CrossRef]

19. Wang, Z.; Jie, Z.; Liu, X. Combustion and Emission Characteristics of Methanol–Diesel Dual Fuel Engine at Different Altitudes. *J. Mar. Sci. Eng.* **2024**, *12*, 2210. [CrossRef]
20. Wang, Y.; Dong, P.; Long, W.; Tian, J.; Wei, F.; Wang, Q.; Cui, Z.; Li, B. Characteristics of Evaporating Spray for Direct Injection Methanol Engine: Comparison between Methanol and Diesel Spray. *Processes* **2022**, *10*, 1132. [CrossRef]
21. Feng, S.; Zhang, S.; Zhang, H.; Shi, J. Effect of nozzle geometry on combustion of a diesel-methanol dual-fuel direct injection engine. *Fuel* **2024**, *357*, 129734. [CrossRef]
22. Zhen, X.; Wang, Y. An overview of methanol as an internal combustion engine fuel. *Renew. Sustain. Energy Rev.* **2015**, *52*, 477–493. [CrossRef]
23. Vancoillie, J.; Sileghem, L.; Van de Ginste, M.; Demuynck, J.; Galle, J.; Verhelst, S. Experimental Evaluation of Lean-Burn and EGR as Load Control Strategies for Methanol Engines. SAE Technical Paper 2012-01-1283. 2012. Available online: <https://www.sae.org/publications/technical-papers/content/2012-01-1283/> (accessed on 20 December 2024).
24. Güdden, A.; Pischinger, S.; Geiger, J.; Heuser, B.; Müther, M. An experimental study on methanol as a fuel in large bore high speed engine applications—Port fuel injected spark ignited combustion. *Fuel* **2021**, *303*, 121292. [CrossRef]
25. Chen, Z.; Wang, L.; Zeng, K. Comparative study of combustion process and cycle-by-cycle variations of spark-ignition engine fueled with pure methanol, ethanol, and n-butanol at various air–fuel ratios. *Fuel* **2019**, *254*, 115683. [CrossRef]
26. Gong, C.; Peng, L.; Chen, Y.; Liu, J.; Liu, F.; Han, Y. Computational study of intake temperature effects on mixture formation, combustion and unregulated emissions of a DISI methanol engine during cold start. *Fuel* **2018**, *234*, 1269–1277. [CrossRef]
27. Duan, Q.; Kou, H.; Li, T.; Yin, X.; Zeng, K.; Wang, L. Effects of injection and spark timings on combustion, performance and emissions (regulated and unregulated) characteristics in a direct injection methanol engine. *Fuel Process. Technol.* **2023**, *247*, 107758. [CrossRef]
28. Li, Y.; Bai, X.S.; Tunér, M.; Im, H.G.; Johansson, B. Investigation on a high-stratified direct injection spark ignition (DISI) engine fueled with methanol under a high compression ratio. *Appl. Therm. Eng.* **2019**, *148*, 352–362. [CrossRef]
29. Zhu, Z.; Mu, Z.; Wei, Y.; Du, R.; Liu, S. Experimental evaluation of performance of heavy-duty SI pure methanol engine with EGR. *Fuel* **2022**, *325*, 124948. [CrossRef]
30. Zhu, Z.; Gu, H.; Zhu, Z.; Wei, Y.; Zeng, K.; Liu, S. Investigation on mixture formation and combustion characteristics of a heavy-duty SI methanol engine. *Appl. Therm. Eng.* **2021**, *196*, 117258. [CrossRef]
31. Sathish Kumar, T.; Ashok, B. Material compatibility of SI engine components towards corrosive effects on methanol-gasoline blends for flex fuel applications. *Mater. Chem. Phys.* **2023**, *296*, 127344. [CrossRef]
32. Schwahn, H.; Lutz, U.; Kramer, U. Deposit Formation of Flex Fuel Engines Operated on Ethanol and Gasoline Blends. SAE Technical Paper 2010-01-1464. 2010. Available online: <https://www.sae.org/publications/technical-papers/content/2010-01-1464/> (accessed on 20 December 2024).
33. Buck, W.H.; Lohuls, J.R.; Murphy, J.A. Lubrication Studies in a Methanol-Fueled Spark Ignition Engine. SAE Technical Paper 892156. 1989. Available online: <https://www.sae.org/publications/technical-papers/content/892156/> (accessed on 20 December 2024).
34. Yuan, B.; Wang, Z.; Cao, J.; Huang, Y.; Shen, Y.; Song, Z.; Zhao, H.; Cheng, X. Mixture formation characteristics and feasibility of methanol as an alternative fuel for gasoline in port fuel injection engines: Droplet evaporation and spray visualization. *Energy Convers. Manag.* **2023**, *283*, 116956. [CrossRef]
35. Han, Z.; Reitz, R.D. Turbulence Modeling of Internal Combustion Engines Using RNG  $\kappa$ - $\epsilon$  Models. *Combust. Sci. Technol.* **1995**, *106*, 267–295. [CrossRef]
36. Beale, J.C.; Reitz, R.D. Modeling spray atomization with the Kelvin-Helmholtz/Rayleigh-Taylor /hybrid model. *At. Sprays* **1999**, *9*, 623–650.
37. He, X.; Xu, K.; Xu, Y.; Zhang, Z.; Wei, W. Effects of nozzle diameter on the characteristic time scales of diesel spray two-stage ignition under cold-start conditions. *Fuel* **2023**, *335*, 126700. [CrossRef]
38. Schmidt, D.P.; Rutland, C.J. A New Droplet Collision Algorithm. *J. Comput. Phys.* **2000**, *164*, 62–80. [CrossRef]
39. O'Rourke, P.J.; Amsden, A.A. A Spray/Wall Interaction Sub-Model for the KIVA-3 Wall Film Model. SAE Technical Paper 2000-01-0271. 2001. Available online: <https://www.sae.org/publications/technical-papers/content/2000-01-0271/> (accessed on 20 December 2024).
40. Xing, K.; Guan, W.; Guo, X.; Wang, Y.; Tu, Z.; Huang, H. Potential of high compression ratio combined with knock suppression strategy for improving thermal efficiency of spark ignition stoichiometric natural gas engine. *Energy Convers. Manag.* **2023**, *276*, 116544. [CrossRef]
41. Chang, W.; Wang, C.; Wu, Y.; Jin, C.; Zhang, Z.; Liu, H. Study on the mechanism of influence of cetane improver on methanol ignition. *Fuel* **2023**, *354*, 129383. [CrossRef]
42. Wu, H.; Dong, X.; Shi, Z.; Li, H.; Cao, W.; Zhang, L.; Bo, Y.; Li, X. Effect of injection timing on knock combustion and pollutant emission of heavy-duty diesel engines at low temperatures. *Chemosphere* **2022**, *305*, 135519. [CrossRef] [PubMed]
43. Yin, X.; Yue, G.; Liu, J.; Duan, H.; Duan, Q.; Kou, H.; Wang, Y.; Yang, B.; Zeng, K. Investigation into the operating range of a dual-direct injection engine fueled with methanol and diesel. *Energy* **2023**, *267*, 126625. [CrossRef]

44. Aniolek, K.; Wilk, R. Pre-flame Oxidation Characteristics of Methanol. *Energy Fuels* **1995**, *9*, 395–405.
45. Zhou, D.Z.; Yang, W.M.; An, H.; Li, J.; Shu, C. A numerical study on RCCI engine fueled by biodiesel/methanol. *Energy Convers. Manag.* **2015**, *89*, 798–807. [[CrossRef](#)]
46. Heywood, J.B. *Internal Combustion Engine Fundamentals*; McGrawHill: New York, NY, USA, 2018.
47. Rakopoulos, D.C.; Rakopoulos, C.D.; Kyritsis, D.C. Butanol or DEE blends with either straight vegetable oil or biodiesel excluding fossil fuel: Comparative effects on diesel engine combustion attributes, cyclic variability and regulated emissions trade-off. *Energy* **2016**, *115*, 314–325. [[CrossRef](#)]

**Disclaimer/Publisher’s Note:** The statements, opinions and data contained in all publications are solely those of the individual author(s) and contributor(s) and not of MDPI and/or the editor(s). MDPI and/or the editor(s) disclaim responsibility for any injury to people or property resulting from any ideas, methods, instructions or products referred to in the content.